ACS APPLIED MATERIALS & INTERFACES

Research Article

www.acsami.org

Synthesis of D-Mannose Capped Silicon Nanoparticles and Their Interactions with MCF-7 Human Breast Cancerous Cells

Jayshree H. Ahire,[†] Isabelle Chambrier,[†] Anja Mueller,[‡] Yongping Bao,[§] and Yimin Chao*,[†]

[†]School of Chemistry, University of East Anglia, Norwich NR4 7TJ, United Kingdom

[‡]School of Pharmacy, University of East Anglia, Norwich NR4 7TJ, United Kingdom

[§]Norwich Medical School, University of East Anglia, Norwich NR4 7TJ, United Kingdom

Supporting Information

ABSTRACT: Silicon nanoparticles (SiNPs) hold prominent interest in various aspects of biomedical applications. For this purpose, surface functionalization of the NPs is essential to stabilize them, target them to specific disease area, and allow them to selectively bind to the cells or the bio-molecules present on the surface of the cells. However, no such functionalization has been explored with Si nanoparticles. Carbohydrates play a critical role in cell recognition. Here, we report the first synthesis of silicon nanoparticles functionalized with carbohydrates. In this study, stable and brightly luminescent D-Mannose (Man) capped SiNPs have been synthesized from amine terminated SiNPs and D-mannopyranoside acid. The surface functionalization is confirmed by Fourier transform infrared spectroscopy (FTIR), nuclear magnetic resonance spectroscopy (NMR), and energy dispersive X-ray spectroscopy (EDX) studies. The mean diameter of the crystal core is 5.5 nm, as measured by transmission electron microscopy (TEM), while the hydrodynamic diameter obtained by dynamic light scattering (DLS) is 16 nm. The quantum yield (QY) of photoluminescence emission is found to be 11.5%, and the nanoparticles exhibit an exceptional stability over two weeks. The Man-capped SiNPs may prove to be valuable tools for further investigating glycobiological, biomedical, and material science fields. Experiments are carried out using Concanavalin A (ConA) as a target protein in order to prove the hypothesis. When Man functionalized SiNPs are treated with ConA, cross-linked aggregates are formed, as shown in TEM images as well as monitored by photoluminescence spectroscopy (PL). Man functionalized SiNPs can target cancerous cells. Visualization imaging of SiNPs in MCF-7 human breast cancer cells shows the fluorescence is distributed throughout the cytoplasm of these cells.

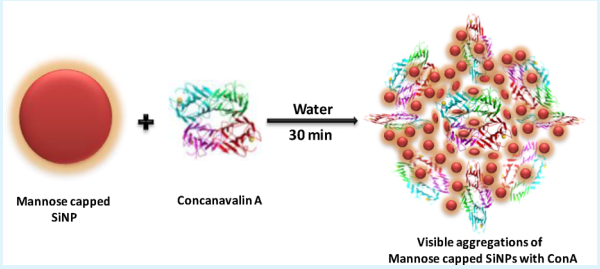

KEYWORDS: *silicon, nanoparticles, D-mannose, protein, fluorescence imaging, cancerous cells*

1. INTRODUCTION

Carbohydrates play a critical role in the process of cell recognition.[1−3] The cell surface is covered with carbohydrates, glycoproteins, and glycolipids. These biomolecules play an important role in the process of cell recognization, cell growth, and inflammatory responses. Carbohydrates mediate cell surface interactions, ranging from interactions with hormones, enzymes, and antibodies to those with bacteria, viruses, and toxins. In addition, carbohydrate surface molecules play an important role in developing vaccines in order to identify, diagnose, and treat. In terms of sensitivity and selectivity, carbohydrates have demonstrated great potential as detection tools.[4−6] At present, carbohydrate functionalized glyconanomaterials are finding many important applications in explaining carbohydrate−protein interactions and cell−cell communication.[3,7−10] In order to determine their biological function, and thus evaluate and design therapeutics, it is vital to identify, quantify, and image carbohydrates, carboproteins, and carbolipids.[11]

Silicon nanoparticles and nanostructures hold prominent interest in various aspects of biomedical research. Current fields of interest range from imaging, detection, and sensing to drug delivery and new therapeutic uses.[12,13] This is in addition to the intrinsic electronic, optical and magnetic properties of the nanostructures. Their fluorescence signatures,[14−16] high quantum efficiency,[17] high brightness,[18] size-dependent tunable light emission,[15,16,19] and great stability versus photobleaching compared to organic dye molecules make them ideal tools for fluorescence imaging.[20,21] These properties have helped to establish silicon nanoparticles as fluorescent cellular markers in a number of diagnostic and assay roles.[22,23] Furthermore, when compared with the heavy elements of several other types of semiconductor quantum dots, silicon generically exhibits negligible toxicity.[22,24−26] Overall, SiNPs have available an array of potential applications thanks to their physical and chemical attributes, including in fields of optoelectronics, thermoelectrics,[27] and bioimaging.[28−30]

Received: May 8, 2013
Accepted: July 2, 2013
Published: July 2, 2013

When considering biomedical applications, surface functionalization of SiNPs is essential in order to target them to specific disease areas and allow them to selectively interact with cells or biomolecules.[31,32] When capped with organic molecules, SiNPs can take their functionality and display a number of interesting additional properties, such as increasing overall stability of NPs, increased solubility, and preventing aggregation and precipitation in a biological environment, all of which are important in biomedical applications. The properties of nanoparticles can be controlled as a result of variation in chemical synthesis methods. The SiNPs external organic shell provides functionality capable of effecting the systems solubility, stability, molecule−molecule interactions and other properties. Bioconjugated nanoparticles are employed in bioimaging applications, including early cancer detection,[33] multiplexed optical coding,[34] signal transduction,[35] sensing,[36] imaging,[1] and in western blot analysis, both *in vivo* and *in vitro*.[37] *In vitro* applications include lactin detection or interaction,[5,6] bacterium detection,[38] cancer cell binding,[23] stem cell monitoring,[39,40] carbohydrate−carbohydrate interaction,[7] carbohydrate−protein and carbohydrate−antibody interaction,[2,8,10] carbohydrate−cell interaction,[41] pathogen and toxin detection,[42] and gene transfer.[43,44] Nanomaterials exhibit a large surface area and also customizable physical properties, including structural stability and novel binding properties. These properties are advantageous in applications such as biodetection and biodiagnostics.[45]

Lin et al. fabricated mannose-coated gold NPs and studied the selective binding to type 1 pili in *Escherichia coli*,[42] which presented a novel method of labelling specific proteins on the cell surface.[46] Syková et al. showed that mannose-modified iron oxide NPs were efficient probes for labelling stem cells.[47] Recently, the Penadés group prepared a small library of multivalent Au-NPs functionalized with different structural fragments of the high mannose undecasaccharide of gp120 in various ligand densities and evaluated their effects on the inhibition of HIV glycoprotein gp120 binding to DC-SIGN expressing cells.[48]

The uptake of NPs functionalized with mannose was reported to be faster than that of unmodified NPs in cancer cells. Such functionalized NPs have also been used efficaciously *in vivo*. ConA is a lectin present in the cell membrane. D-Mannose has strong binding affinity towards ConA and thus interacts easily with molecules located on the cell membrane.

Here, we demonstrate a simple room-temperature, two-step synthesis of Man-capped SiNPs that exhibit strong blue photoluminescence when dissolved in water, as well as giving a strong orange luminescence when in the dry state. The Man-capped silicon nanoparticles are synthesized from amine terminated SiNPs,[49] by using N,N′-dicyclohexylcarbodiimide (DCC) as a coupling agent. The resulting SiNPs are pure, stable, and show a very bright luminescence at room temperature. The biochemical activity of Man-capped SiNPs is tested with ConA. The visualized photoluminescence images of SiNPs in MCF-7 human breast cancerous cells are also shown.

2. EXPERIMENTAL METHODS

2.1. Synthesis Method of D-Mannose Terminated Silicon Nanoparticles. Highly stable amine capped SiNPs were synthesized using a previously reported method.[49] A D-mannopyranosyl acid (30 mg, 0.078 mmol) and *N,N′*-dicyclohexylcarbodiimide (DCC) (18 mg, 1.1 equiv, 0.085 mmol) were dissolved in dichloromethane (10 ml) and left, with stirring, for 1 h at room temperature. Freshly prepared amine terminated SiNPs (10 mg) were then added into the reaction mixture and stirred for 24 h at room temperature. The reaction mixture was washed with water (3 × 10 mL) and extracted into CH_2Cl_2. The mixture was dried with Na_2SO_4, and solvent was removed under vacuum. Deacetylation of Man-capped SiNPs was performed in sodium methoxide in methanol and then stirred with $[H^+]$ resin.

2.2. Transmission Electron Microscopy (TEM) and Dynamic Light Scattering (DLS) Measurements. TEM measurement was carried out using a JEOL JEM-2000 Ex microscope and HRTEM was measured with a Philips CM200 FEGTEM microscope. TEM samples were prepared by dipping a carbon-coated 200 mesh copper grid into a solution of redissolved Man-capped SiNPs in DI water. After the solvent evaporated, TEM images were obtained from different spots of each grid.

DLS measurement was recorded with a Zetasizer Nano ZS (Malvern Instruments Ltd., U.K.). Man-capped silicon nanoparticles were redissolved in DI water and the hydrodynamic diameters were obtained at room temperature.

2.3. Fourier Transform Infrared (FTIR), NMR, and Energy Dispersive X-ray Spectroscopy (EDX). FTIR spectra (Perkin Elmer FTIR spectrometer 100) were obtained from a solid sample of Man-capped SiNPs. The sample was placed on the ATR crystal and 36 scans were taken with the background subtracted.

^1H NMR and ^{13}C NMR spectra of Man-capped SiNPs in D_2O and $CDCl_3$ were recorded on a Bruker (Top Spin 3.1, 500 MHz) spectrometer. The Man-capped SiNPs were dried under vacuum and re-dissolved in D_2O or $CDCl_3$, as required.

The EDX measurement was done using EDX sensor attached to a JEOL scanning electron microscope (SEM). The sample was coated with gold (Au), which was used as a reference.

2.4. UV−Vis Absorption and Photoluminescence Spectroscopy. UV−vis absorption spectra were recorded using a Perkin Elmer 35 UV−vis double-beam spectrophotometer in a quartz cuvette (10 × 10 mm). Spectra were recorded by scanning over a 300−700 nm range at a rate of 480 nm per min and were corrected by subtracting the background contribution from the dispersing solvent. The PL spectra were recorded using a Perkin Elmer LS55 spectrophotometer with an excitation slit width of 10 nm and an emission slit width set at 5 nm. The excitation wavelength was fixed at 360 nm. The emission spectra were corrected using the solvent emission as background.

The quantum yield of the Man-capped SiNPs was calculated with eq 1:

$$Q = Q_R\left(\frac{\text{Grad}}{\text{Grad}_R}\right)\left(\frac{\eta^2}{\eta_R^2}\right) \quad (1)$$

where Q is the quantum yield and Grad is the gradient from a plot of integrated fluorescence intensity against absorbance. The subscript R refers to the reference fluorophore of known quantum yield. Here, quinine sulphate was used as reference, which has a quantum yield of 54.6% when dissolved in 1 N H_2SO_4. 1 N (0.5 M) H_2SO_4 had a refractive index η_R of 1.346, while the refractive index η of water was 1.33.

2.5. Live Cell Imaging. The human breast cancer cell line MCF-7 was chosen as one of the targeting cells by Man-capped SiNPs. The cells were seeded on a sterile coverslip in a 6-well plate and grown at 37°C under a 5% CO_2 atmosphere for 12 h in DMEM supplemented with 10% FCS, 2 mM L-glutamine, 1× non-essential amino acids, and 1× penicillin/streptomycin. The growth medium was then removed and replaced with fresh medium, and nanoparticles were added to a final concentration of 50 μg mL^{-1}. The cells were subsequently incubated for 48 h; then, the medium was removed, the cells were washed with PBS three times and were then mounted onto glass slide and then imaged using an inverted Leica DMII fluorescence microscope. To visualize the lysosomes, cells were stained with Lysotracker-Red (Invitrogen), according to manufacturers protocols.

3. RESULTS AND DISCUSSION

3.1. Synthesis of D-Mannose Capped Silicon Nanoparticles. The Man-capped SiNPs were synthesized with D-mannose; see Scheme 1. First, the D-mannose was protected with acetate (OAc) groups to form D-mannose pentaacetate (**1a**). The 1-allyl-2,3,4,6-tetra-O-acetyl-D-mannopyranoside (**1b**) was formed by allylation synthesis of (**1a**), accomplished according to the literature, followed by the isolation of pure anomers.[50] Then, **1b** derivatives were further oxidized to carboxylic acids to form the acid functionalized 2,3,4,6-tetra-O-acetyl-D-mannopyranosyl acid (**1c**).

Scheme 1. Schematic Representation of Synthesis of D-Mannose Capped SiNPs

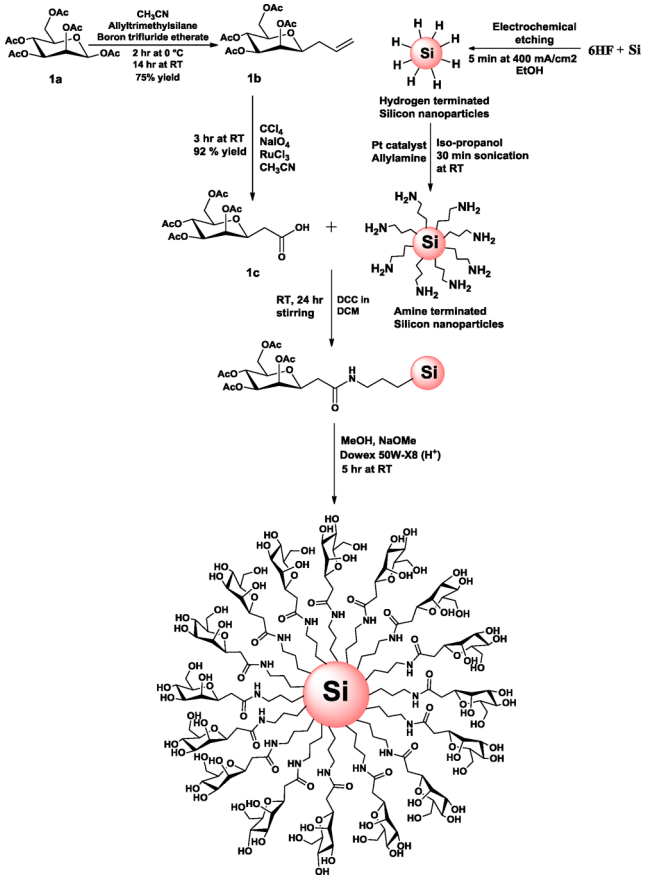

The amine terminated silicon nanoparticles were synthesized using the method described in our previous paper.[49] The amine terminated SiNPs were purified and reacted with D-mannopyranosyl acid in the presence of DCC as a coupling agent.

The time required for the reaction is 24 h. The obtained crude reaction mixture, i.e. the intermediate, was washed three times with water in order to remove the unreacted amine terminated SiNPs. After washing, the remaining reaction mixture was left with DCC and the by-product urea, which is difficult to remove at this stage because this by-product, as well as the DCC and OAc-Man-capped SiNPs are soluble in dichloromethane. Deacetylation of the reaction mixture removes the acetate group of the Man-capped SiNPs and offers hydroxyl Man-capped SiNPs, which are soluble in water. In order to obtain a pure product, the mixture was washed with dichloromethane to remove DCC and urea. A pinkish solid product of the pure D-mannose-capped SiNPs (typically 40 mg) was obtained after deacetylation of each crude reaction mixture. This sticky solid was re-dissolved in water for further characterization.

3.2. Size Measurement with TEM and DLS. The size and size distribution of Man-capped SiNPs were examined by TEM and DLS. Prior to the measurements the sticky solid powder of pure Man-capped SiNPs was dissolved in water. Figure 1a shows a TEM image of Man-capped SiNPs on a carbon coated copper grid.

The histogram in Figure 1b shows the size distribution of Man-capped SiNPs. The TEM measurement showed that the mean size and size distribution of Man-capped SiNPs is 5.5 ± 2.4 nm after analyzing 195 nanoparticles from different regions of the grid. The inset in Figure 1a shows the highly crystalline structure of the atomic lattices. The lattice spacing of 0.31 nm is

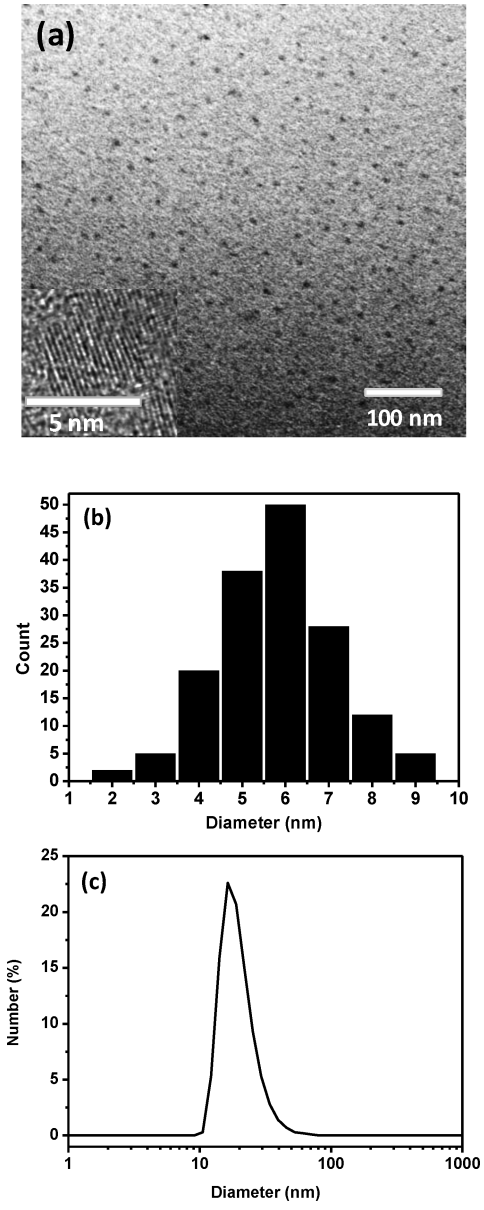

Figure 1. (a) TEM image of Man-capped SiNPs and inset showing a high resolution TEM image of an individual silicon nanocrystal screening the crystal lattice planes. (b) Histogram showing size distribution of Man-capped SiNPs. (c) DLS spectrum displaying the size and size distribution of Man-capped silicon nanoparticles in water.

dx.doi.org/10.1021/am4017126 | ACS Appl. Mater. Interfaces 2013, 5, 7384−7391

consistent with the Si (111) plane. DLS results of Man-capped SiNPs show that the peak diameter is 16 nm; see Figure 1c. This size is larger than the one obtained from TEM measurements because the Mannose ligand around the silicon nanoparticles form a hydration shell, whereby DLS measures the hydrodynamic diameter of the Man-capped SiNPs in water.[5,11,51,52]

3.3. Chemical Bonding and Elemental Analysis. In Figure S1 in the Supporting Information, the EDX analysis shows all the elements in the expected functionalities in their expected ratios. The SiNPs surface is coated with a large number of carbon and oxygen atoms in agreement with this analysis, where the highest peak was carbon and the second highest peak oxygen, which are present in the D-mannose groups as well as in the Si−O bonding. In addition, there is a sharp peak of silicon, which is indicative of the core. Overall, the analysis proves that not only is the surface functionalized with D-mannose but also the silicon core nanoparticles are present in the sample.

Confirmation that the SiNPs surface is covered with D-mannose through amide bond formation was obtained from FTIR spectra, acquired in normal transmission alignment. Figure 2 compares the FTIR spectrum of the Man-capped

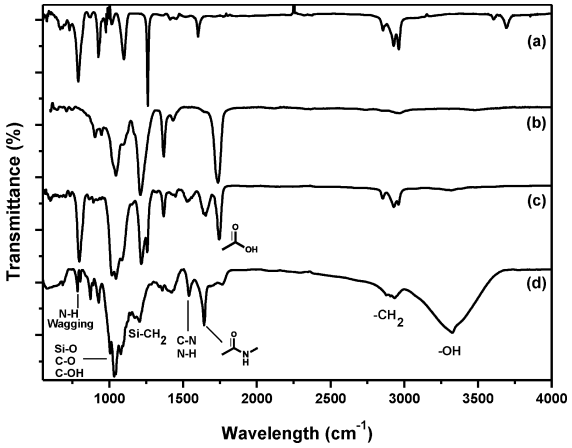

Figure 2. FTIR spectra of (a) amine terminated SiNPs, (b) D-mannopyranosyl acid **1c**, (c) intermediate OAc-Man-capped SiNPs, (d) pure Man-capped SiNPs at solid state (32 scans, 2 cm^{-1} resolution).

SiNPs produced in this work (Figure 2d) with those obtained for the starting amine terminated SiNPs (Figure 2a) and D-mannopyranosyl acid **1c** (Figure 2b) as well as that of the intermediate OAc protected Man-capped SiNPs. All spectra were obtained from dry solid samples.

The FTIR spectrum of Man-capped SiNPs (Figure 2d) shows a broad peak at 3300−3625 cm^{-1} attributed to vibrations of the four −OH groups of the mannose moiety. The N−H stretching of the amide function observed in the spectrum of the intermediate OAc-protected Man-capped SiNPs (Figure 2c) in the same region is evidently not visible due to overlap. However, the peak at 1551 cm^{-1} is attributed to the C−N stretching and N−H bending from the amide group, and this is only observed in the intermediate OAc-Man-capped SiNPs (Figure 2c) and the product (Figure 2d) spectra. The broad amide N−H wagging band is observed at 737 cm^{-1}. Further evidence for the amide link arises from the presence of a sharp band at 1654 cm^{-1}, which is attributed to the C═O stretching of the amide carbonyl, and this is not seen in the D-mannopyranosyl acid sugar **1c** (Figure 2b) whose C═O acid vibration exhibits a peak at 1725 cm^{-1}. Further features observed around 2853−2961 cm^{-1} are attributed to the C−H stretching of the alkane chains. These peaks lose some of their intensity in the product (Figure 2d) relative to the intermediate (Figure 2c) due to the removal of the acetate protecting groups (OAc). The bands in the spectrum (Figure 2c) at 1450 cm^{-1} and 1258 cm^{-1} are attributed to Si−CH_2 vibrational scissoring and symmetric bending respectively. These are less visible in Figure 2d due to the effect of an oxide peak at 1100 cm^{-1}. The spectrum in Figure 2c shows two peaks at 1258 cm^{-1} and 1217 cm^{-1}, which correspond to Si−CH_2 symmetric bending and C−O bond of the Mannose moiety, respectively, which is also apparent in the starting material (Figure 2b). The peak observed at 1369 cm^{-1} is assigned to the C−O−C group of the Man sugar, which can also be observed in spectra shown in Figure 2b, c, and d. The broad band observed at 1008−1062 cm^{-1} is attributed to Si−O, C−O, and C−OH. The broadening and the high intensity of this peak are due to the four hydroxyl OH groups of the Mannose and not to the Si−O bond, which can be clearly seen in both spectra in Figure 2c and d.

All these observed features confirm that the SiNPs are capped with Mannose sugar molecules. Also, these characteristics highlight the strength and stability of the Si−C bond formed between the SiNPs and the Man sugar, as well as a minimal number of Si−OR surface bonds present.

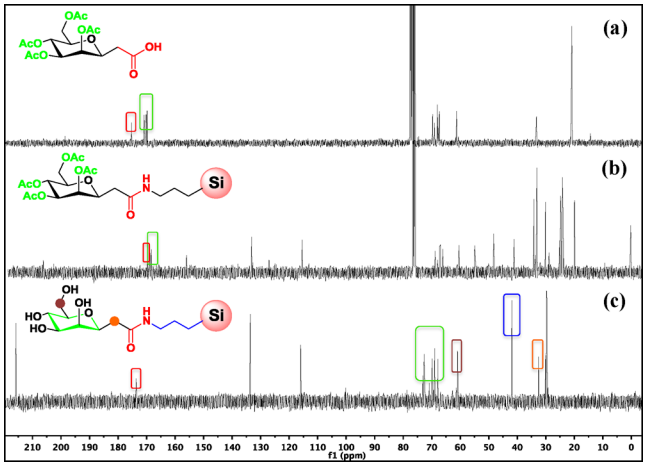

Figure 3. ^{13}C NMR spectra of (a) D-mannopyranosyl acid **1c** in $CDCl_3$, (b) intermediate OAc-Man-capped silicon nanoparticles in $CDCl_3$, and (c) pure Man-capped SiNPs in D_2O.

The surface chemical bonding of Man-capped SiNPs was also confirmed by ^{13}C NMR spectroscopy. Figure 3 compares the ^{13}C NMR spectra of D-mannopyranosyl acid **1c** (starting material) in $CDCl_3$, intermediate OAc protected Man-capped SiNPs in $CDCl_3$ and Man-capped SiNPs in D_2O. Unfortunately, it was not possible to obtain all three spectra in the same solvent due to the differing solubilities of the various compounds.

The spectrum of D-mannopyranosyl acid **1c** (Figure 3a) shows a peak at 175.79 ppm, which is attributed to the carbonyl (—C═O) of the acid function of Man sugar. The four peaks between 169.6 ppm to 170.6 ppm are attributed to the four OAc protecting groups of Man sugar. The five carbon atoms

dx.doi.org/10.1021/am4017126 | ACS Appl. Mater. Interfaces 2013, 5, 7384−7391

making up the carbohydrate ring have peaks located at 67 ppm to 69.4 ppm. The peaks at 61 ppm and 33 ppm are attributed to the two $-CH_2$ groups of Man sugar. The formation of the amide bond is clearly observable in intermediate OAc-Man-capped SiNPs (Figure 3b) through the disappearance of the acid carbon peak at 175.79 ppm and the appearance of a new peak at 169.76 ppm, attributed to the amide carbonyl carbon. The spectrum in Figure 3b is that of a crude sample due to the complexity of isolation (see the experimental section) and shows peaks in the aliphatic region belonging to reagents and side-products. Following the removal of the acetate groups, the spectrum of Man-capped SiNPs (Figure 3c) shows only a single peak in the carbonyl region at 173 ppm attributed to the amide carbonyl carbon. The peaks at 115.72 ppm and 133.4 ppm belong to the amine capped nanoparticles. The peaks at 215 ppm and 29 ppm originate from acetone-d_6, which was added as reference to the tube in D_2O.

3.4. Photoluminescence (PL) and Quantum Yield (QY). The absorption and emission spectra of aqueous Man-capped SiNPs are presented in Figure 4a. The inset photograph shows the Man-capped SiNPs in water under UV illumination at 364 nm. The gradual increase in the absorbance with decreasing excitation wavelength from the onset wavelength of 450 nm, corresponding to the absorption edge of 2.75 eV, is characteristic of absorption across silicon's indirect band gap.[14] The PL spectrum of room temperature aqueous Man-capped SiNPs is shown as the solid line. The maximum emission peak is centred at 468 nm with a full width at half maximum (FWHM) of 58 nm under an excitation wavelength of 360 nm.

Interestingly the PL of Man-capped SiNPs in solid phase, where the sample was drop cast onto a glass coverslip and dried *in vacuo*, shows a strong orange luminescence under UV light. The PL emission spectrum of Man-capped SiNPs in solid phase is presented in Figure 4b, with an inset showing a photograph of the Man-capped SiNPs under UV illumination of 254 nm. The maximum emission peak, under an excitation wavelength of 360 nm, is centered at 600 nm, and the second peak is centered at 476 nm, with a FWHM of 51 nm and 56 nm, respectively. In Figure 4a and b, the peak centered at 468 nm is characteristic of absorption across the band gap of silicon and is thus responsible for blue emission; in Figure 4b, the peak centered at 600 nm shows orange emission, a consequence of surface states and defects due to surface functionality. In the solid phase, both components are observable, but the orange emission peak centered at 600 nm is not present in the solution. This suggests the quenching effect of solvent around the surface functionality of SiNPs. It is the surface functionality that causes this change in luminescence, the hydroxyl $-OH$ groups on the Mannose sugar molecule form hydrogen bonds with the solvent, which causes the quenching of the orange emission.

Quantum yield (QY) of aqueous Man-capped SiNPs were measured with quinine sulfate (QY = 54.6%) as a reference emitter;[53] see Figure 5. An aqueous solution of Man-capped SiNPs with absorbance between 0.1 and 0.01 was prepared, and the gradient of the integrated fluorescence intensities against absorbance was found. The QY of Man-capped SiNPs was found to be 11.5 % with an excitation wavelength at 360 nm. The obtained QY in aqueous solution is comparable to those reported before,[20,23] ranging from 2 to 18% in water.

For silicon nanoparticles, a limiting factor is the insufficiency of PL stability for potential biological applications. To investigate the PL stability, time-dependent PL spectra were measured on Man-capped SiNPs in water (Figure S2, Supporting Information) and in the dry state (Figure 6) by

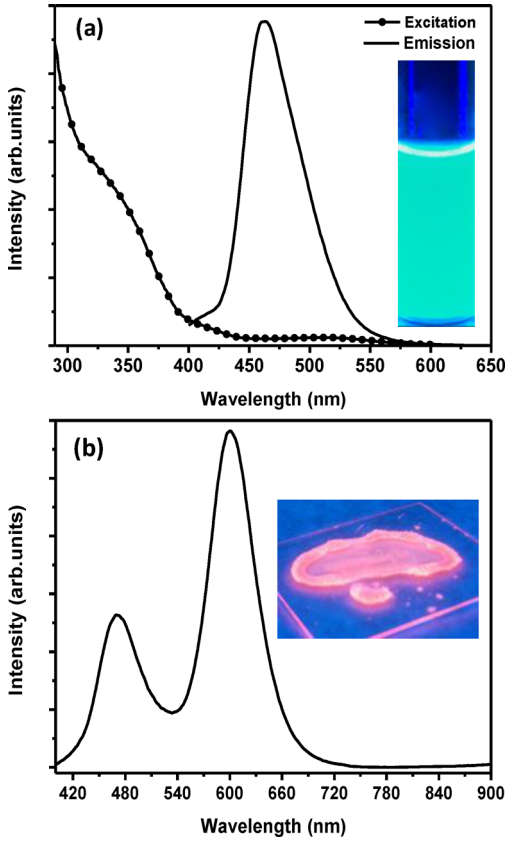

Figure 4. (a) The solid line shows the photoluminescence spectrum of aqueous Man-capped SiNPs under an excitation of 360 nm; the dotted line shows the absorption spectrum of aqueous Man-capped SiNPs; the inset photo shows the photoluminescence from aqueous Man-capped SiNPs under a UV lamp. (b) The photoluminescence spectrum of Man-capped SiNPs in solid state under an excitation of 360 nm. The inset photo shows the photoluminescence from a dry sample of Man-capped SiNPs under a UV lamp.

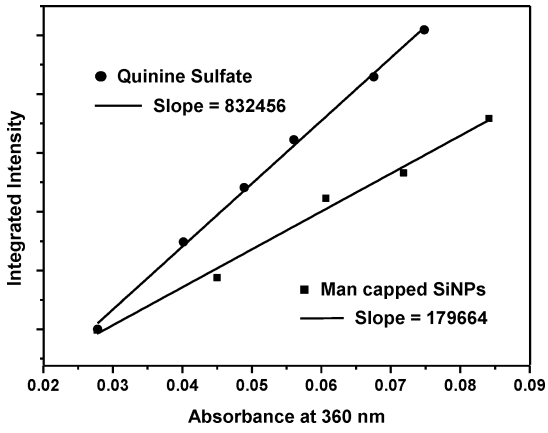

Figure 5. Integrated PL intensity versus absorbance for multiple diluted Man-capped SiNPs in water and for various dilution of quinine sulfate in 0.5 M H_2SO_4 under identical excitation conditions.

dx.doi.org/10.1021/am4017126 | ACS Appl. Mater. Interfaces 2013, 5, 7384−7391

monitoring the PL emission using an excitation wavelength of 360 nm.

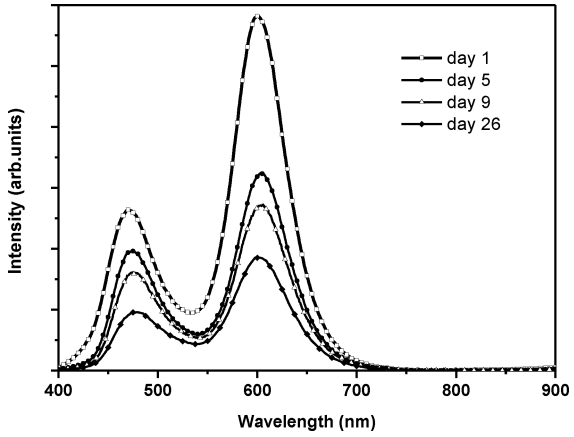

Figure 6. Ageing effect of a dry sample of Man-capped SiNPs by PL at an excitation wavelength of 360 nm.

Figure 6 shows the PL stability of a dry sample of Man-capped SiNPs. It is observed that the PL emission remains visible for over a month. Figure S6 (Supporting Information) shows the PL stability of Man-capped SiNPs in water, it clearly shows that the sample is stable for over two months if kept in the dark.[5]

3.5. Biochemical Activity. Biochemical activity of the Man-capped SiNPs was tested using ConA (Figure 7). ConA is

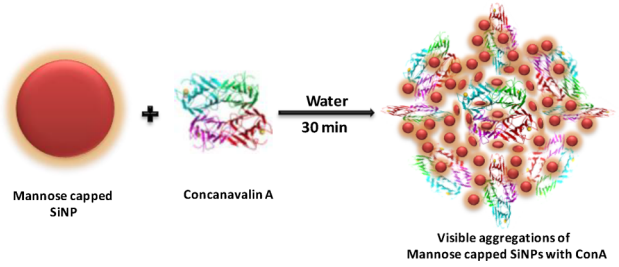

Figure 7. Graphical representation of agglutination of Man-capped SiNPs by ConA tetramer in water.

a lectin, which has strong binding specificity toward mannose and weak binding affinity towards galactose.[54] One ConA contain four mannose binding sites that can cross link to multiple mannose functionalized SiNPs, leading to the nanoparticles aggregation, which results in the reduction of emission at 464 nm, and aggregation can also be seen in the TEM image . As a proof of principle, this process was examined by PL (Figure 8a) and TEM images (Figure 8b)

Upon the addition of ConA to Man-capped SiNPs, visible aggregates of particles were observed within a minute. This aggregation is associated with a significant reduction in the intensity of the luminescence peak at 464 nm (Figure 8a). The suspended aggregates gradually precipitated out of solution. After approximately 4 h all of the nanoparticle systems had completely precipitated, as shown by the gradual decreasing PL intensity with increasing time in Figure 8a. The Man-capped SiNPs were also examined by TEM before and after ConA addition. Before ConA addition, the NPs were highly dispersed, (Figure 1a), whereas large aggregates were formed after ConA addition (Figure 8b).

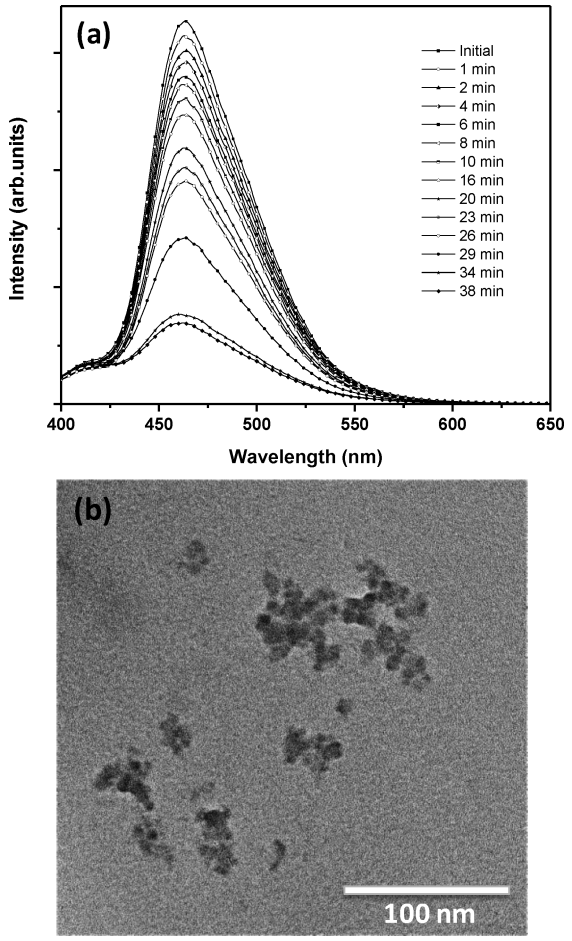

Figure 8. (a) Aggregations of Man-capped SiNPs with Con A was monitored by PL spectroscopy. (b)TEM image of Man-capped SiNPs after addition of Con A.

3.6. Targeting Cancerous Cells. It is well known that Mannose has a strong binding affinity towards lactin,[55] which is present on the surface of cell and is also well characterized with *Escherichia coli* system.[4,56] After successfully detecting lactin, we evaluated the effectiveness of Man-capped SiNPs in mammalian cell interaction and cancer cell detection. Antibodies can be used to detect particular antigens. However, some mutant cancer cells lack these markers. Also, antibodies can only bind to specific cell surface biomolecules. In contrast, carbohydrates can interact with a multitude of cells and impart information regarding carbohydrate receptors, therefore limiting the number of possible reagents.[57] MCF-7, a human breast cancer cell line, was chosen as the targeting cells by Man-capped SiNPs. In a non-cancerous cell line, galactoside binding galactines-4, -7, and -8 are absent. However, these galactines are present in the MCF-7 cancer cells.[58]

Fluorescence microscope images are shown in Figure 9. The control image of MCF-7 cells without incubation of SiNPs is shown in Figure 9a. Bright fluorescence has arisen from the emission of SiNPs, see Figure 9b. In order to visualize the lysosomes, cells were stained with Lysotracker-Red, see Figure 9c. The merged results are also shown in Figure 9d. The selective uptake and intracellular accumulation of Man-capped SiNPs in MCF-7 cells is clearly observed and thus can lead to the further development of Man-capped SiNPs as a vehicle for

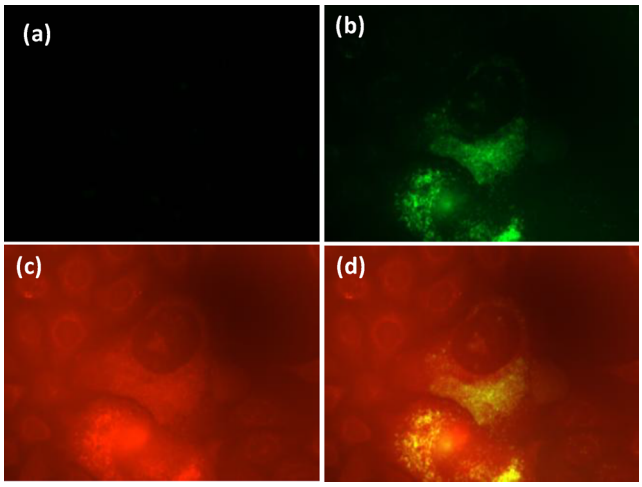

Figure 9. Fluorescence images inside living MCF-7 cancerous cells: (a) control; (b) fluorescence from Man-capped SiNPs inside the cells after 48 h incubation; (c) after 48 h Lysotracker stain; (d) merged image. Pictures were taken on live cells using a Leica fluorescence microscope.

targeted drug delivery.[59] Importantly, morphological damage to aqueous Man-capped SiNP treated cells cannot be observed.

The strongly binding Man-capped SiNPs were found to be internalized by the breast cancer cells. Although only one tumor cell line was used in this study, there might be still the possibility that Man-capped SiNPs bind to other cancerous cell lines if there are similar receptors located on the surface of these cells. The research is still in progress using different types of tumor cells and testing them with Man-capped SiNPs.

4. CONCLUSIONS

A simple method has been demonstrated to synthesize highly pure and stable Man-capped SiNPs through the utilisation of amine terminated SiNPs. The SiNPs capped with Man sugar show strong blue photoluminescence under UV excitation in water and strong orange photoluminescence in the solid state, with a QY of 11.5 %. These surface functionalized nanoparticles are stable against degradation over several weeks. The FTIR and NMR spectra obtained display the surface functionalization, confirming that the surface is effectively modified with Man sugar. The EDX confirmed the makeup of the core shell of silicon nanoparticles as well as the overall chemical composition. The biochemical activity of highly pure Man-capped SiNPs were tested with ConA. As an example, the SiNPs targeting MCF-7 has been investigated under the fluorescence microscope. The present work not only has implications in the area of surface functionalization of SiNPs but also has a broad potential to allow for study of various further applications, with considerable interest in both medicine and biology. Our understanding of cancer cell functions, such as endocytosis, cell−matrix and cell−cell communications, can be greatly enhanced by studying carbohydrate-receptor functions as a result of Man-capped SiNP utilization. In addition, such studies can help further understanding of specificity and ligand optimization. In the future, this increasing knowledge base will enhance the applications of Man-capped SiNPs for *in vivo* cancer detection.[57]

■ ASSOCIATED CONTENT

Supporting Information

Synthesis of amine-capped SiNPs; general procedure for allylation of mannose pentaacetate (**1a**); general procedure for oxidation of 1-allyl-2,3,4,6-tetra-O-acetyl-D-mannose-pyranosides (**1b**); deacetylation of OAc-protected Man-capped SiNPs; EDX measurements; quantum yield measurement; ageing effect of Mannose capped SiNPs by PL; aggregation experiment of amine capped SiNPs with ConA monitored by PL. This material is available free of charge via the Internet at http://pubs.acs.org

■ AUTHOR INFORMATION

Corresponding Author

*E-mail: y.chao@uea.ac.uk.

Author Contributions

The manuscript was written through contributions of all authors. All authors have given approval to the final version of the manuscript.

Notes

The authors declare no competing financial interest.

■ ACKNOWLEDGMENTS

J.H. Ahire is grateful to a Tyndall studentship and an ORS award. This research is supported by EPSRC under grant number EP/G01664X/1. Mr. Jason Thomas is thanked for critical proof reading and discussions.

■ REFERENCES

(1) Michalet, X.; Pinaud, F. F.; Bentolila, L. A.; Tsay, J. M.; Doose, S.; Li, J. J.; Sundaresan, G.; Wu, A. M.; Gambhir, S. S.; Weiss, S. *Science* **2005**, *307*, 538−544.
(2) Kikkeri, R.; Lepenies, B.; Adibekian, A.; Laurino, P.; Seeberger, P. H. *J. Am. Chem. Soc.* **2009**, *131*, 2110−2012.
(3) Lis, H.; Sharon, N. *Chem. Rev.* **1998**, *98*, 637−674.
(4) El-Boubbou, K.; Zhu, D. C.; Vasileiou, C.; Borhan, B.; Prosperi, D.; Li, W.; Huang, X. *J. Am. Chem. Soc.* **2010**, *132*, 4490−4499.
(5) Babu, P.; Sinha, S.; Surolia, A. *Bioconjugate Chem.* **2007**, *18*, 146−151.
(6) Dam, T. K.; Brewer, C. F. *Chem. Rev.* **2002**, *102*, 387−430.
(7) Ratner, D. M.; Adams, E. W.; Disney, M. D.; Seeberger, P. H. *ChemBioChem* **2004**, *5*, 1375−1383.
(8) Oh, E.; Lee, D.; Kim, Y.-P.; Cha, S. Y.; Oh, D.-B.; Kang, H. A.; Kim, J.; Kim, H.-S. *Angew. Chem. Int. Ed.* **2006**, *45*, 7959−7963.
(9) Lindhorst, T. K. *Essentials of Carbohydrate Chemistry and Biochemistry*; Wiley-VCH: Weinheim, 2003.
(10) Lee, Y. C.; Lee, R. T. *Acc. Chem. Res.* **1995**, *28*, 321−327.
(11) Earhart, C.; Jana, N. R.; Erathodiyil, N.; Ying, J. Y. *Langmuir* **2008**, *24*, 6215−6219.
(12) O'Farrell, N.; Houlton, A.; Horrocks, B. R. *Int. J. Nanomed.* **2006**, *1*, 451−472.
(13) Wang, Q.; Ni, H.; Pietzsch, A.; Hennies, F.; Bao, Y.; Chao, Y. *J. Nanopart. Res.* **2011**, *13*, 405−413.
(14) Sato, S.; Swihart, M. T. *Chem. Mater.* **2006**, *18*, 4083−4088.
(15) Belomoin, G.; Therrien, J.; Smith, A.; Rao, S.; Twesten, R.; Chaieb, S.; Nayfeh, M. H.; Wagner, L.; Mitas, L. *Appl. Phys. Lett.* **2002**, *80*, 841−843.
(16) English, D. S.; Pell, L. E.; Yu, Z.; Barbara, P. F.; Korgel, B. A. *Nano Lett.* **2002**, *2*, 681−685.
(17) Rogozhina, E. V.; Eckhoff, D. A.; Gratton, E.; Braun, P. V. *J. Mater. Chem.* **2006**, *16*, 1421−1430.
(18) Rogozhina, E.; Belomoin, G.; Smith, A.; Abuhassan, L.; Barry, N.; Akcakir, O.; Braun, P. V.; Nayfeh, M. H. *Appl. Phys. Lett.* **2001**, *78*, 3711−3713.

(19) Schuppler, S.; Friedman, S. L.; Marcus, M. A.; Adler, D. L.; Xie, Y. H.; Ross, F. M.; Chabal, Y. J.; Harris, T. D.; Brus, L. E.; Brown, W. L.; Chaban, E. E.; Szajowski, P. F.; Christman, S. B.; Citrin, P. H. *Phys. Rev. B* **1995**, *52*, 4910.
(20) Warner, J. H.; Hoshino, A.; Yamamoto, K.; Tilley, R. D. *Angew. Chem. Int. Ed.* **2005**, *44*, 4550−4554.
(21) Rosso-Vasic, M.; Spruijt, E.; van Lagen, B.; De Cola, L.; Zuilhof, H. *Small* **2008**, *4*, 1835−1841.
(22) Mayne, A. H.; Bayliss, S. C.; Barr, P.; Tobin, M.; Buckberry, L. D. *Phys. Status Solidi A* **2000**, *182*, 505−513.
(23) Erogbogbo, F.; Yong, K.-T.; Roy, I.; Xu, G.; Prasad, P. N.; Swihart, M. T. *ACS Nano* **2008**, *2*, 873−878.
(24) Nilsson, J. R. *Acta Protozool.* **2003**, *42*, 19−29.
(25) Kirchner, C.; Liedl, T.; Kudera, S.; Pellegrino, T.; Muñoz Javier, A.; Gaub, H. E.; Stölzle, S.; Fertig, N.; Parak, W. J. *Nano Lett.* **2004**, *5*, 331−338.
(26) Wang, Q.; Bao, Y.; Ahire, J.; Chao, Y. *Adv. Health. Mater.* **2013**, *2*, 459−465.
(27) Ashby, S.; García-Cañadas, J.; Min, G.; Chao, Y. *J. Electron. Mater.* **2013**, *42*, 1495−1498.
(28) Miller, D. A. B. *Nature* **1995**, *378*, 238.
(29) Alsharif, N. H.; Berger, C. E. M.; Varanasi, S. S.; Chao, Y.; Horrocks, B. R.; Datta, H. K. *Small* **2009**, *5*, 221−228.
(30) Arya, H.; Kaul, Z.; Wadhwa, R.; Taira, K.; Hirano, T.; Kaul, S. C. *Biochem. Biophys. Res. Commun.* **2005**, *329*, 1173−1177.
(31) Erogbogbo, F.; Tien, C.-A.; Chang, C.-W.; Yong, K.-T.; Law, W.-C.; Ding, H.; Roy, I.; Swihart, M. T.; Prasad, P. N. *Bioconjugate Chem.* **2011**, *22*, 1081−1088.
(32) Sailor, M. J.; Park, J.-H. *Adv. Mater.* **2012**, *24*, 3779−3802.
(33) Wu, X.; Liu, H.; Liu, J.; Haley, K. N.; Treadway, J. A.; Larson, J. P.; Ge, N.; Peale, F.; Bruchez, M. P. *Nat. Biotechnol.* **2003**, *21*, 41−46.
(34) Han, M.; Gao, X.; Su, J. Z.; Nie, S. *Nat. Biotechnol.* **2001**, *19*, 631−635.
(35) Lidke, D. S.; Nagy, P.; Heintzmann, R.; Arndt-Jovin, D. J.; Post, J. N.; Grecco, H. E.; Jares-Erijman, E. A.; Jovin, T. M. *Nat. Biotechnol.* **2004**, *22*, 198−203.
(36) Medintz, I. L.; Clapp, A. R.; Mattoussi, H.; Goldman, E. R.; Fisher, B.; Mauro, J. M. *Nat. Mater.* **2003**, *2*, 630−638.
(37) Zhelev, Z.; Bakalova, R.; Ohba, H.; Jose, R.; Imai, Y.; Baba, Y. *Anal. Chem.* **2005**, *78*, 321−330.
(38) Liu, L.-H.; Dietsch, H.; Schurtenberger, P.; Yan, M. *Bioconjugate Chem.* **2009**, *20*, 1349−1355.
(39) Shi, Z.; Neoh, K. G.; Kang, E. T.; Shuter, B.; Wang, S.-C.; Poh, C.; Wan, W. *ACS Appl. Mater. Interfaces* **2009**, *1*, 328−335.
(40) Lu, C.-W.; Hung, Y.; Hsiao, J.-K.; Yao, M.; Chung, T.-H.; Lin, Y.-S.; Wu, S.-H.; Hsu, S.-C.; Liu, H.-M.; Mou, C.-Y.; Yang, C.-S.; Huang, D.-M.; Chen, Y.-C. *Nano Lett.* **2007**, *7*, 149−154.
(41) Nolting, B.; Yu, J.-J.; Liu, G.-y.; Cho, S.-J.; Kauzlarich, S.; Gervay-Hague, J. *Langmuir* **2003**, *19*, 6465−6473.
(42) Lin, C.-C.; Yeh, Y.-C.; Yang, C.-Y.; Chen, C.-L.; Chen, G.-F.; Chen, C.-C.; Wu, Y.-C. *J. Am. Chem. Soc.* **2002**, *124*, 3508−3509.
(43) Ahmed, M.; Deng, Z.; Liu, S.; Lafrenie, R.; Kumar, A.; Narain, R. *Bioconjugate Chem.* **2009**, *20*, 2169−2176.
(44) de la Fuente, M.; Seijo, B.; Alonso, M. J. *Gene Ther.* **2008**, *15*, 668−676.
(45) Rosi, N. L.; Mirkin, C. A. *Chem. Rev.* **2005**, *105*, 1547−1562.
(46) Macher, B. A.; Galili, U. *Biochim. Biophys. Acta* **2008**, *1780*, 75−88.
(47) Horák, D.; Babič, M.; Jendelová, P.; Herynek, V.; Trchová, M.; Pientka, Z.; Pollert, E.; Hájek, M.; Syková, E. *Bioconjugate Chem.* **2007**, *18*, 635−644.
(48) Martínez-Ávila, O.; Hijazi, K.; Marradi, M.; Clavel, C.; Campion, C.; Kelly, C.; Penadés, S. *Chem.—Eur. J.* **2009**, *15*, 9874−9888.
(49) Ahire, J. H.; Wang, Q.; Coxon, P. R.; Malhotra, G.; Brydson, R.; Chen, R.; Chao, Y. *ACS Appl. Mater. Interfaces* **2012**, *4*, 3285−3292.
(50) Kramer, J. R.; Deming, T. J. *J. Am. Chem. Soc.* **2010**, *132*, 15068−15071.
(51) Kumar, C. G.; Mamidyala, S. K.; Reddy, M. N.; Reddy, B. V. S. *Process Biochem.* **2012**, *47*, 1488−1495.
(52) Wang, Q.; Bao, Y.; Zhang, X.; Coxon, P. R.; Jayasooriya, U. A.; Chao, Y. *Adv. Health. Mater.* **2012**, *1*, 189−198.
(53) Xiong, H. M.; Wang, Z. D.; Xia, Y. Y. *Adv. Mater.* **2006**, *18*, 748−751.
(54) Shimura, K.; Kasai, K. *Anal. Biochem.* **1995**, *227*, 186−194.
(55) Jiang, X.; Housni, A.; Gody, G.; Boullanger, P.; Charreyre, M.-T. R. S.; Delair, T.; Narain, R. *Bioconjugate Chem.* **2010**, *21*, 521−530.
(56) El-Boubbou, K.; Gruden, C.; Huang, X. *J. Am. Chem. Soc.* **2007**, *129*, 13392−13393.
(57) Wang, X.; Liu, L.-H.; Ramström, O.; Yan, M. *Exp. Biol. Med.* **2009**, *234*, 1128−1139.
(58) Chandrasekaran, S.; Tanzer, M. L.; Giniger, M. S. *J. Biol. Chem.* **1994**, *269*, 3367−3373.
(59) Yamazaki, N.; Kojima, S.; Bovin, N. V.; André, S.; Gabius, S.; Gabius, H. J. *Adv. Drug Delivery Rev.* **2000**, *43*, 225−244.